
Neural Topographic Factor Analysis for fMRI Data

Eli Sennesh^{*1,3}, Zulqarnain Khan^{*2}, Yiyu Wang³
 Jennifer Dy², Ajay Satpute³, J. Benjamin Hutchinson⁴, Jan-Willem van de Meent¹
 sennesh.e@northeastern.edu, khan.zu@ece.neu.edu, wang.yiyu@northeastern.edu
 jdy@ece.neu.edu, a.satpute@northeastern.edu, bhutch@uoregon.edu,
 j.vandemeent@northeastern.edu

¹ Khoury College of Computer Sciences, Northeastern University

² Department of Electrical and Computer Engineering, Northeastern University

³ Department of Psychology, Northeastern University

⁴ Department of Psychology, University of Oregon

Abstract

Neuroimaging studies produce gigabytes of spatio-temporal data for a small number of participants and stimuli. Rarely do researchers attempt to model and examine how individual participants vary from each other – a question that should be addressable even in small samples given the right statistical tools. We propose Neural Topographic Factor Analysis (NTFA), a probabilistic factor analysis model that infers embeddings for participants and stimuli. These embeddings allow us to reason about differences between participants and stimuli as signal rather than noise. We evaluate NTFA on data from an in-house pilot experiment, as well as two publicly available datasets. We demonstrate that inferring representations for participants and stimuli improves predictive generalization to unseen data when compared to previous topographic methods. We also demonstrate that the inferred latent factor representations are useful for downstream tasks such as multivoxel pattern analysis and functional connectivity.

1 Introduction

Analyzing functional neuroimaging studies is both a large data problem and a small data problem. A single scanning run typically comprises hundreds of full-brain scans that each consist of tens of thousands of spatial locations (known as voxels). At the same time, neuroimaging studies tend to have limited statistical power [Cremers et al., 2017]; a typical study considers a cohort of 20-50 participants undergoing tens of stimuli from ten (or fewer) stimulus categories. This poses a significant problem for the over fourteen-thousand functional neuroimaging studies that seek to address both fundamental and translational research questions in cognitive neuroscience on individual differences in functional neural activity [Elliott et al., 2020]. A largely unsolved challenge in this domain is to develop analysis methods that appropriately account for both the commonalities and variations among participants and stimuli effects, scale to tens of gigabytes of data, and reason about uncertainty.

In this paper, we develop Neural Topographic Factor Analysis (NTFA)², a generative model for neuroimaging data that explicitly represents variation among participants and stimuli. NTFA extends Topographic Factor Analysis (TFA) and Hierarchical Topographic Factor Analysis (HTFA) [Manning et al., 2014b, 2018]. It differs from these models in that it learns a prior that maps embeddings (i.e. vectors of features) for each participant and stimulus to a conditional distribution over spatial factors and weights, instead of imposing a single global prior. The result is a structured probabilistic model that learns a representation of each participant and each stimulus.

*Equal contribution

²Source code submitted with paper and available upon request.

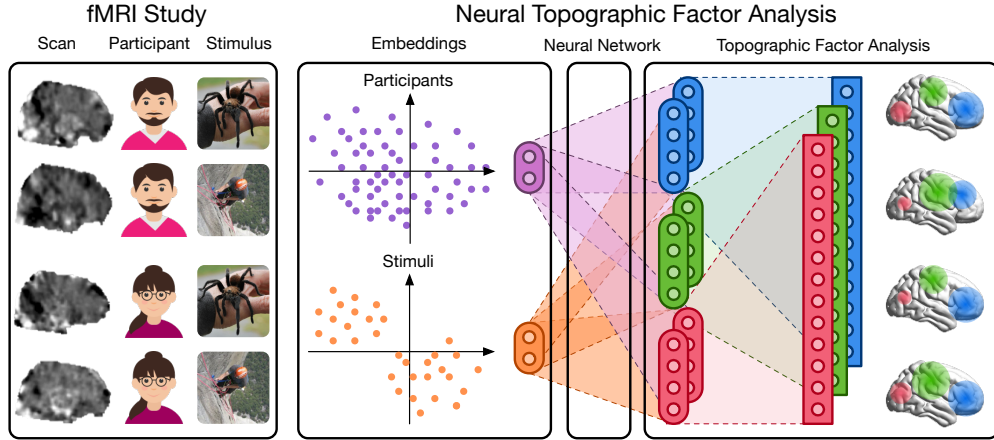


Figure 1: **Overview of Neural Topographic Factor Analysis (NTFA)**: We decompose the fMRI signal into Gaussian factors (shown in red, green and blue in the figure) that correspond to spatially and temporally related brain activity across individuals. A typical fMRI study consists of multiple trials of participants undergoing scans while experiencing different stimuli (or performing different tasks). In our generative model we represent these participants (purple) and stimuli (orange) with embedding vectors. A multilayer perceptron then predicts the factors’ location, size, and weights.

NTFA offers two advantages over other dimensionality reduction methods that project data into a low-dimensional space: Our embeddings factorize the generative contributions of participants from those of stimuli, and they supply uncertainty measures by which we can measure the scale of the embedding space. Having the embedding space “scaled” by uncertainty allows us more confidence in resolving differences: if the means for embeddings of stimuli lie several standard deviations apart from each other, we can be confident they reflect significant differences in the neural response.

We perform a qualitative evaluation of inferred embeddings on four datasets:

- We show that in a synthetic dataset, simulated from distinguishable clusters of participants and stimuli, inference recovers the underlying cluster structure.
- We present results for our own pilot study investigating whether threat-relevant stimuli from three categories induce the same or different patterns of neural response. NTFA infers stimulus embeddings that show differences in patterns of neural response between stimulus categories.
- We analyze and evaluate two publicly available datasets. In the first, participants with major depressive disorder and controls listened to emotionally valenced sounds and music [Lepping et al., 2016]. In the second, participants viewed images of faces, cats, five categories of man-made objects, and scrambled pictures [Haxby et al., 2001]. In both cases, NTFA infers an embedding structure that is consistent with previously reported findings.

Because NTFA is, to our knowledge, the first model to explicitly infer embeddings for participants and stimuli, we devise two simple baselines as comparisons. The first is to apply PCA directly to the input data, and the second is to compute post-hoc embeddings after training a shared response model (SRM) [Chen et al., 2015]. PCA fails to recover participant and stimulus structure, whereas the SRM yields point-estimates that are qualitatively similar but lack uncertainty estimates.

As a sanity check, we also compare predictive performance on a validation set of brain images across NTFA and HTFA. We hold out trials by their stimulus-participant pairs, requiring our model to generalize from other trials in which the same stimulus or participant were seen. PCA, the SRM, and TFA cannot recombine representations to predict such novel combinations in this way.

This work makes both neuroscientific and machine learning contributions. From a machine learning perspective, NTFA is a novel neural extension of probabilistic factor analysis methods. The inferred embeddings capture similarities in the neural response across participants and stimuli. This improves prediction on held-out data, while requiring fewer trainable parameters. From a neuroscientific perspective, the generative model in NTFA contributes to our ability to characterize individual variation in whole-brain analyses. Psychological states (e.g. emotions and memories) involve patterns of activation distributed widely throughout voxel space [Haxby et al., 2001, Satpute and Lindquist, 2019]. Existing whole-brain analyses such as multivoxel pattern analysis (MVPA) thus often rely on

Table 1: Comparison of factor analysis methods for fMRI data. When a method considers participant and stimulus variations dependently, we consider it to model variation in the independent factor. Our method (NTFA) is shown in the bottom row.

Model	Spatial factors	Participant variation	Stimulus variation	Scanning run variation
PCA	✗	✗	✗	✗
SRM	✗	✓	✗	✓
TFA	✓	✗	✗	✗
HTFA	✓	✗	✗	✓
TLSA	✓	✓	✗	✗
NTFA	✓	✓	✓	✓

supervised feature selection using labels for stimulus categories or participant groups [Pereira et al., 2009]. In contrast, latent factors from NTFA and HTFA enable unsupervised whole-brain MVPA, and can be used to create data-driven functional connectomes.

Figure 1 outlines our proposed approach. Section 2 covers related work in factor analysis for neuroimaging data, primarily the spatially topographic methods on which we build. Section 3 develops the NTFA model. Section 4 discusses our architectural details, preprocessing steps, and experiments, then discusses and evaluates experimental results. Section 5 concludes.

2 Background

Factor analysis methods are widely used to reduce the dimensionality of neuroimaging data. These methods decompose the fMRI signal for a trial $Y \in \mathbb{R}^{T \times V}$ with T time points and V voxels into a product $Y \simeq WF$ between a lower-rank matrix of weights $W \in \mathbb{R}^{T \times K}$ and a lower-rank matrix of factors $F \in \mathbb{R}^{K \times V}$. The dimension $K \ll V$ is chosen to balance the degree of dimensionality reduction and the reconstruction accuracy.

Standard methods that are applied primarily to fMRI data include Principal Component Analysis [Abdi and Williams, 2010] and Independent Component Analysis [Hyvärinen et al., 2001]. There are also methods that have been specifically developed for fMRI analysis. These include adaptations of dictionary learning methods for large-scale fMRI datasets [Mensch et al., 2017], hyper-alignment (HA) [Haxby et al., 2011], the shared response model (SRM) [Chen et al., 2015] and the matrix-normal shared response model (MN-SRM) [Shvartsman et al., 2018] for functional alignment, as well as topographic latent source analysis (TLSA) [Gershman et al., 2011, 2014], topographic factor analysis [Manning et al., 2014b], and hierarchical topographic factor analysis [Manning et al., 2014a, 2018] for functional connectivity. Many of these come in probabilistic varieties [Cai et al., 2020].

Topographic models define spatially smooth factors via radial basis functions. Non-topographical models - such as PCA, ICA, the SRM, the MN-SRM and dictionary learning - learn a $V \times K$ factor-voxel loading matrix³, with no requirement of spatial smoothness. Some of these learn factor-loading weights for participants, such as the SRM, while others such as dictionary learning learn factor-loading weights for experimental conditions or stimuli. HA can be considered a special case of the SRM with $K = V$. The MN-SRM is also very similar to the SRM except it enforces a weaker Gaussianity constraint on the factor-loading weights instead of the orthonormality constraint in SRM. Table 1 compares our model’s latent factorization structure to those of other models. NTFA is novel in learning independent low-dimensional embeddings for both participants and stimuli.

2.1 Topographic Factor Analysis

This work extends TFA and HTFA, two probabilistic models that employ radial basis functions to represent spatial factors. TFA and HTFA model data that comprises N trials (i.e. continuous recordings), each of which contain T time points for voxels at V spatial positions. TFA approximates each trial separately $Y_n \simeq W_n F_n$ as a product between time-varying weights $W_n \in \mathbb{R}^{T \times K}$ and spatially-varying factors $F_n \in \mathbb{R}^{K \times V}$. To do so, TFA assumes that the data is noisily sampled from

³In some cases for each subject, requiring a total of VKP parameters to be learned for a study with P participants, or each stimulus, requiring VKS parameters, where K is the number of factors and S is the number of unique stimuli.

the inner product between the weights and factors matrices

$$Y_n \sim \mathcal{N}(W_n F_n, \sigma^Y). \quad (1)$$

TFA combines this likelihood $p(Y_n | W_n, F_n)$ with the prior $p(W_n, F_n)$ to define a probabilistic model $p(Y_n, W_n, F_n)$. Black-box methods are then used to approximate the posterior $p(W_n, F_n | Y_n)$ with a mean-field variational distribution $q_\lambda(F_n, W_n)$ on the factors W_n and F_n .

The prior $p(W_n, F_n) = p(W_n) p(F_n)$ factorizes over W_n and F_n . The prior over weights $p(W_n)$ is a hierarchical Gaussian with hyperparameters $\mu_{n,k}^W$ and $\sigma_{n,k}^W$,

$$W_{n,t,k} \sim \mathcal{N}(\mu_{n,k}^W, \sigma_{n,k}^W), \quad \mu_{n,k}^W \sim p(\mu^W), \quad \sigma_{n,k}^W \sim p(\sigma^W), \quad (2)$$

To define a prior over factors $p(F_n)$, TFA employs a kernel function that ensures spatial smoothness of factor values $F_{n,k,v}$ at nearby voxel positions $x_v^G \in \mathbb{R}^3$. This kernel function κ is normally a radial basis function (RBF), which models each factor $k \in \{1 \dots K\}$ as a Gaussian with center at a spatial location $x_{n,k}^F \in \mathbb{R}^3$, whose width is determined by the kernel hyper-parameters $\rho_{n,k}^F$,

$$F_{n,k,v} = \kappa(x_v^G, x_{n,k}^F; \rho_{n,k}^F), \quad x_{n,k}^F \sim p(x^F), \quad \rho_{n,k}^F \sim p(\rho^F). \quad (3)$$

Interpreting factor analysis generatively enables us to incorporate additional assumptions to capture similarities across a set of related trials. HTFA [Manning et al., 2014a, 2018], introduces variables \bar{x}_k^F and $\bar{\rho}_k^F$ representing each factor’s mean positions and widths across trials,

$$x_{n,k}^F \sim p(x_{n,k}^F | \bar{x}_k^F), \quad \bar{x}_k^F \sim p(\bar{x}^F), \quad \rho_{n,k}^F \sim p(\rho_{n,k}^F | \bar{\rho}_k^F), \quad \bar{\rho}_k^F \sim p(\bar{\rho}^F). \quad (4)$$

HTFA assumes that brain layouts and activations across trials vary around a shared Gaussian prior. This imposes unimodality upon the distribution of neural responses across trials.

3 Neural Topographic Factor Analysis

NTFA extends TFA to model variation across participants and stimuli. We assume the same factor analysis model as TFA, which approximates the fMRI signal as a linear combination of time-dependent weights and spatially varying Gaussian factors. NTFA extends TFA by inferring *embedding vectors* for individual participants and stimuli. We learn a mapping from embeddings to the parameters of the likelihood model, parameterized by a neural network. Instead of HTFA’s global template, we introduce factorized latent spaces of participant and stimulus embeddings, and share the neural networks mapping embeddings to factors. For reference, a complete description of our notation can be found in Table 3 in the Appendix.

The advantage of incorporating neural networks into the generative model is that it enables us to explicitly reason about multimodal response distributions and effects that vary between individual samples. The network weights θ are shared across trials, as are the stimulus and participant embeddings z_s^S and z_p^P . This allows NTFA to capture statistical regularities within a whole experiment. At the same time, the use of neural networks ensures that differences in embeddings can be mapped onto a wide range of spatial and temporal responses. Whereas the hierarchical Gaussian priors in HTFA implicitly assume that response distributions are unimodal and uncorrelated across different factors $k \in [K]$, the neural network in NTFA can model such correlations by jointly predicting all K factors.

We model N trials in which participants $p_n \in \{1, \dots, P\}$ undergo a set of stimuli $s_n \in \{1, \dots, S\}$ and are scanned for T time points per trial. We assume that participant embeddings $\{z_1^P, \dots, z_P^P\}$ and stimulus embeddings $\{z_1^S, \dots, z_S^S\}$ are shared across trials. For simplicity, we will consider the case where both embeddings have the same dimensionality D and a Gaussian prior

$$z_p^P \sim \mathcal{N}(0, I), \quad z_s^S \sim \mathcal{N}(0, I). \quad (5)$$

For each participant p , we define the RBF center x_p^F and log-width ρ_p^F in terms of a neural mapping

$$x_p^F \sim \mathcal{N}(\mu_p^x, \sigma_p^x), \quad \mu_p^x, \sigma_p^x \leftarrow \eta_\theta^{F,x}(z_p^P), \quad (6)$$

$$\rho_p^F \sim \mathcal{N}(\mu_p^\rho, \sigma_p^\rho), \quad \mu_p^\rho, \sigma_p^\rho \leftarrow \eta_\theta^{F,\rho}(z_p^P). \quad (7)$$

Here η_θ^F is a neural network parameterized by a set of weights θ , which models how variations between participants and stimuli affect the factor positions and widths in brain activations. This network outputs a $K \times 4 \times 2$ tensor, that contains a two-tuple of three-dimensional parameters for

Algorithm 1 NeuralTFA Generative Model

(p_1, \dots, p_N)	▷ Participant for each trial
(s_1, \dots, s_N)	▷ Stimulus for each trial
1: for p in $1, \dots, P$ do	
2: $z_p^p \sim \mathcal{N}(0, I)$	▷ Equation (5)
3: for s in $1, \dots, S$ do	
4: $z_s^s \sim \mathcal{N}(0, I)$	▷ Equation (5)
5: for n in $1, \dots, N$ do	
6: $p, s \leftarrow p_n, s_n$	
7: $(\mu_p^x, \sigma_p^x), (\mu_p^\rho, \sigma_p^\rho) \leftarrow \eta_\theta^F(z_p^p)$	
8: $x_p^F \sim \mathcal{N}(\mu_p^x, \sigma_p^x)$	▷ Equation (6)
9: $\rho_p^F \sim \mathcal{N}(\mu_p^\rho, \sigma_p^\rho)$	▷ Equation (7)
10: $\mu_n^w, \sigma_n^w \leftarrow \eta_\theta^W(z_p^p, z_s^s)$	▷ Equation (8)
11: for t in $1 \dots T$ do	
12: $W_{n,t} \sim \mathcal{N}(\mu_n^w, \sigma_n^w)$	▷ Equation (8)
13: $F_p \leftarrow \kappa(x_p^F, \rho_p^F)$	
14: $Y_{n,t} \sim \mathcal{N}(W_{n,t} \cdot F_p, \sigma^Y)$	▷ Equation (9)

each factor center (μ_p^x, σ_p^x) and another two-tuple of one-dimensional parameters for each factor log-width $(\mu_p^\rho, \sigma_p^\rho)$. We use a second network $\eta_\theta^W(z_p^p, z_s^s)$ to parameterize the distribution over weights $W_{n,t}$ with a $K \times 2$ tensor, given the embeddings for each trial n and time point t with $p = p_n, s = s_n$:

$$W_{n,t} \sim \mathcal{N}(\mu_n^w, \sigma_n^w), \quad \mu_n^w, \sigma_n^w \leftarrow \eta_\theta^W(z_p^p, z_s^s). \quad (8)$$

The likelihood model is the same as that in TFA,

$$Y_{n,t} \sim \mathcal{N}(W_{n,t} \cdot F_p, \sigma^Y), \quad F_p \leftarrow \kappa(x_p^F, \rho_p^F). \quad (9)$$

We summarize the generative model for NTFA in Algorithm 1. This model defines a joint density $p_\theta(Y, W, x^F, \rho^F, z^p, z^s)$, which in turn defines a posterior $p_\theta(W, x^F, \rho^F, z^p, z^s | Y)$ when conditioned on Y . We approximate the posterior with a fully-factorized variational distribution,

$$q_\lambda(W, \rho^F, x^F, z^p, z^s) = \prod_{n,t} q_{\lambda_{n,t}^w}(W_{n,t}) \prod_s q_{\lambda_s^s}(z_s^s) \prod_p q_{\lambda_{x_p^F}}(x_p^F) q_{\lambda_{\rho_p^F}}(\rho_p^F) q_{\lambda_p^p}(z_p^p). \quad (10)$$

We learn the parameters θ and λ by maximizing the evidence lower bound (ELBO)

$$\mathcal{L}(\theta, \lambda) = \mathbb{E}_q \left[\log \frac{p_\theta(Y, W, x^F, \rho^F, z^p, z^s)}{q_\lambda(W, x^F, \rho^F, z^p, z^s)} \right] \leq \log p_\theta(Y).$$

We optimize this objective using black-box methods provided by Probabilistic Torch, a library for deep generative models that extends the PyTorch deep learning framework [Narayanaswamy et al., 2017]. Specifically, we maximize an importance-weighted bound [Burda et al., 2016] using a doubly-reparameterized gradient estimator [Tucker et al., 2019]. This objective provides more accurate estimates for the gradient of the log marginal likelihood.

While neural network models can have thousands or even millions of parameters, we emphasize that NTFA in fact has a *lower* number of trainable parameters than HTFA. This follows from the fact that TFA and HTFA assume fully-factorized variational distributions that have $O(NK + NTK)$ parameters for N trials with T time points. In NTFA, the networks η^F and η^W have $O(D(D + K))$ parameters each, whereas the variational distribution has $O(D(P + S) + PK + NTK)$ parameters.

In practice, scanning time limitations impose a trade-off between N and T . For this reason NTK does not always dominate NK , since often $T \propto O(10)$. We can then choose $D \propto O(1)$ and $K \propto O(100)$, and if we label constant factors c , the total number of parameters becomes $O(cD^2 + cDK)$, making $O(cDK)$ the dominant term. When $P \ll N$, as is usually the case, NTFA can therefore have orders of magnitude fewer parameters than HTFA for $D = 2$.

4 Evaluation

4.1 Datasets

We consider four datasets in our experiments. First, we create a simulated dataset to verify that NTFA can recover a ground-truth structure in data that, by construction, contains clearly distinguishable

participant and stimulus clusters (labelled ‘‘Synthetic’’). Second, we analyze a previously unpublished data from a pilot study, conducted by one of the authors, that measures the neural response to threat-relevant stimuli (labelled ‘‘ThreatVids’’). Third, we analyze a publicly available dataset on valenced sounds and music, with participants divided into a control group and a depressed group [Lepping et al., 2016] (labelled ‘‘Lepping’’). Finally, we verify that NTFA can reconstruct a popular publicly available dataset of participants watching pictures of animate and inanimate objects [Haxby et al., 2001] (labelled ‘‘Haxby’’). These experimental datasets vary in their number of participants, time points, voxels, and task variables. A detailed description of each of these datasets can be found in Appendix A.5, and our standard neuroimaging preprocessing pipeline is discussed in Appendix A.6.

4.2 Model Architecture and Training

We employ participant and stimulus embeddings with $D = 2$ in all experiments. For the synthetic dataset, we analyze the data with the same number of factors as were used to generate it, $K = 3$. For non-simulated data we use $K = 100$ factors. This is somewhat fewer than previously reported for HTFA ($K = 700$) [Manning et al., 2018] owing to GPU memory limitations. We report parameter counts for HTFA and NTFA in Table 2, and provide details on network architectures in Appendix A.7.

4.3 Generalization to Held-out Images

To evaluate generalization, we split datasets into training and test sets, ensuring the training set contains at least one trial for each participant $p \in \{1, \dots, P\}$ and each stimulus $s \in \{1, \dots, S\}$. To do so, we construct a matrix of $(p, s) \in \{1, \dots, P\} \times \{1, \dots, S\}$ with participants as rows and stimuli as columns. We then choose all trials along the matrix’s diagonals $\{n : p_n \bmod S = s_n\}$ as our test set. All other trials are used as the training set.

We evaluate generalization to held-out data in terms of the posterior-predictive probability

$$p_\theta(\tilde{Y} | Y) = \int p_\theta(\tilde{Y} | z^p, z^s) p_\theta(z^p, z^s | Y) dz^p dz^s.$$

Like the marginal likelihood, this quantity is intractable. We approximate it by computing a VAE-style lower bound $\mathbb{E}[\tilde{\mathcal{L}}] \leq \log p_\theta(\tilde{Y} | Y)$ from L samples (see Appendix A.4 for a derivation),

$$\tilde{\mathcal{L}} = \frac{1}{L} \sum_{l=1}^L \log p(\tilde{Y} | \tilde{W}^{(l)}, \tilde{x}^F^{(l)}, \tilde{\rho}^F^{(l)}, z^p^{(l)}, z^s^{(l)}). \quad (11)$$

We sample embeddings from the variational distribution and remaining variables from the prior

$$z^p^{(l)} \sim q(z^p), \quad z^s^{(l)} \sim q(z^s), \quad \tilde{W}^{(l)}, \tilde{x}^F^{(l)}, \tilde{\rho}^F^{(l)} \sim p_\theta(\tilde{W}, \tilde{x}^F, \tilde{\rho}^F | z^p^{(l)}, z^s^{(l)}).$$

In Table 2, we compare NTFA to HTFA in terms of log predictive probability for held-out data, computing an importance-weighted bound over each dataset’s test set. Across datasets, NTFA exhibits a higher log-likelihood and log-predictive probability than HTFA, with the same number ($K = 100$) of latent factors. We observe larger improvements by NTFA over HTFA in datasets such as ThreatVids, in which NTFA shares statistical strength across trials since $N \gg P$ and $N \gg S$.

We visualize the posterior-predictive means for held-out trials in Appendix A.3. HTFA shares its predictive distribution across all trials, because it lacks any explicit representation of participants and stimuli. By contrast, NTFA’s predictive representation more closely resembles the actual data.

Table 2: **Generalization performance** (in log predictive probability) and **parameter counts**. We approximate the log predictive with a VAE-style lower bound. We evaluate on a test set of held out subject-stimuli pairs, and use $K = 100$ factors across datasets and models. For NTFA we set $D = 2$.

	Log-predictive HTFA	Log-predictive NTFA	Parameter count HTFA	Parameter count NTFA
Synthetic ($K = 3$)	-4.72×10^6	-4.68×10^6	2.16×10^4	1.90×10^4
ThreatVids	-2.23×10^9	-2.19×10^9	1.64×10^8	8.88×10^6
Lepping	-2.54×10^9	-2.47×10^9	2.53×10^7	2.61×10^6
Haxby	-7.17×10^8	-7.10×10^8	1.44×10^6	1.01×10^6

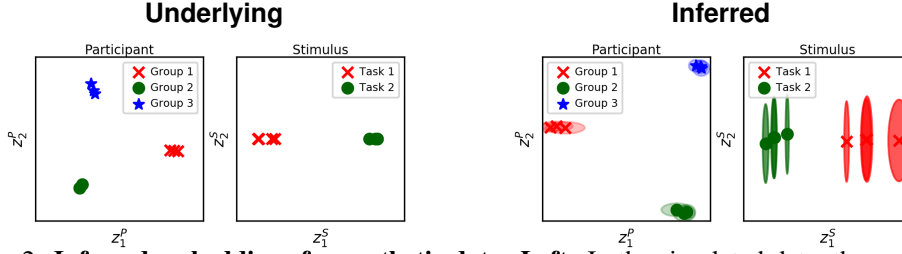


Figure 2: **Inferred embeddings for synthetic data:** **Left:** In the simulated data, three groups of participants exhibit varying levels of response in three different brain regions to *Task 1* and *Task 2* stimuli, depending on the locations of underlying participant and stimulus embeddings used to generate the data. **Right:** NTFA recovers these conditions in participant and stimulus embeddings without prior knowledge. Only the relative spatial arrangement is of interest. Since the original embeddings vary relative to each other only along the horizontal axis, NTFA learns a distribution for these embeddings with very high variance along the vertical axis.

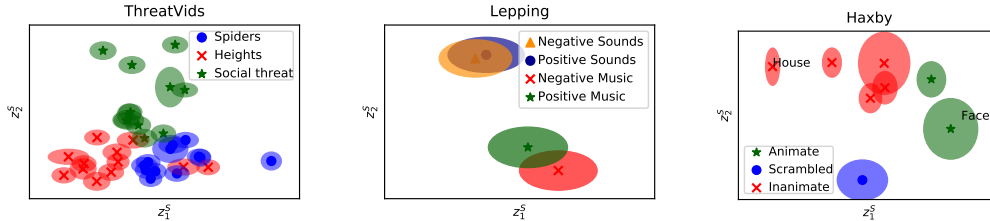


Figure 3: **Inferred distributions of stimulus embeddings.** **Left:** On ThreatVids, stimulus embeddings recovered groups of fear stimuli. **Middle:** On the Lepping dataset, stimulus embeddings clearly distinguish the musical stimuli from the non-musical sounds; positive vs negative music show less overlap than positive vs negative sounds. **Right:** On the Haxby dataset, stimulus embeddings for animate objects are separated from various inanimate objects. Faces were among the animate embeddings and clearly distinct from the embedding for houses, as expected [Haxby et al., 2001].

4.4 Inferred Embeddings

NTFA infers embeddings for both participants and stimuli, along with estimates of uncertainty for those embeddings. Participant embeddings appeared to primarily reflect idiosyncratic differences among participants, without mapping clearly to any participant conditions or behavior available in the datasets. We discuss these participant embeddings in detail in Appendix A.1. Here we discuss the extent to which stimulus embeddings align with with experimenter-defined categories.

Synthetic Data: For synthetic data, NTFA recovers stimulus and participant embeddings that are qualitatively similar to the embeddings that we used to generate the data (Figure 2). We emphasize that embeddings are learned directly from the synthetic data in an entirely unsupervised manner, which means that there is in principle no reason to expect embeddings to be exactly the same. However, we do observe that learned embeddings for participants and stimuli are well-separated, appear to have some variance, and are invariant under linear transformations. Moreover, given the “true” number of factors ($K = 3$), NTFA reconstructs synthetic data better than HTFA.

ThreatVids Dataset: In this dataset, metadata provided individual stimulus labels as well as stimulus categories to group them together. Table 2 shows that NTFA generalizes better than HTFA to held-out participant-stimulus pairs, without additional inference. In an analysis without resting-state data, NTFA uncovers stimulus embeddings that clearly correlate with stimulus categories. While “Heights” and “Spiders” show some overlap, “Social Threat” is clearly separated (Figure 3, left column).

Lepping Dataset: We here infer one embedding per stimulus category, since the metadata does not label individual stimuli. The embeddings (Figure 3, middle column) display a clear separation between music and nonmusical sounds, with positive and negative music showing a greater probability of differing from one-another. Positive and negative sounds overlap in the embedding space. This is consistent with previous findings [Lepping et al., 2016].

Haxby Dataset: We here again infer category embeddings. Inference resulted in stimulus embeddings spread throughout the embedding space, with animate and inanimate stimuli segregated (Figure 3,

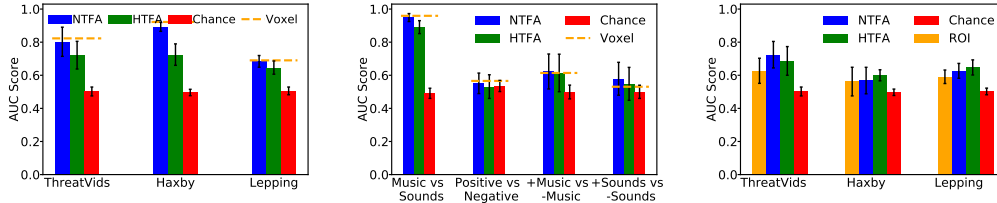


Figure 4: **Classification performance** measured by Accuracy Under the Curve (AUC). We show mean AUC scores with 95% CI across categories. **Left:** For each dataset, we compare supervised voxel selection (“Voxel”), NTFA and HTFA. **Middle:** AUC scores for Lepping dataset across different stimulus categories. The embeddings in Figure 3 (middle) qualitatively match these results. **Right:** Classification using pairwise time-correlation matrices. Functional connectomes derived from NTFA and HTFA’s representations outperform those from the data-agnostic regions of interest (ROIs).

right column). This reflects the evidence for distinct processing of animate and inanimate objects in scenes [Naselaris et al., 2012, Blumenthal et al., 2018].

4.5 Point-estimate Embeddings from the SRM, the MN-SRM and PCA

Evaluating the results above poses inherent challenges in the sense that we lack ground truth. Moreover, NTFA is, to our knowledge the first method that infers low-dimensional embeddings for participants and stimuli directly from the data. To provide some point of comparison, we devise two ad-hoc baselines that compute point estimates of embeddings directly from the input data.

The first baseline applies PCA, to see how a simple model might still capture meaningful structure in embeddings. We vectorized each trial Y_n to obtain N vectors of TV dimensions. We then time-averaged these vectors, performed PCA upon them, and retained the first two principal components. This linear projection of the data did not capture any meaningful structure, as shown in Figure 9 in Appendix A.2.

The second baseline computes post-hoc embeddings from the SRM. The SRM learns a shared response matrix $S \in \mathbb{R}^{T \times K}$ and a participant-specific orthonormal weight matrix $W_p \in \mathbb{R}^{K \times V}$ to approximate the signal as $S \cdot W_p$. Since our datasets comprise unaligned stimuli, we reorder blocks in each scanning run to align stimuli across participants. We then compute participant embeddings by vectorizing the W_p and projecting to the first two principal components with PCA. We split the shared-response matrix S into stimulus blocks S_s and then project to the first two principal components. We show results for this analysis in Figure 7 and Figure 10 in Appendix A.2.

The third baseline computes post-hoc embeddings from the Matrix Normal SRM in exactly the same fashion as done for SRM. The MN-SRM is similar to the SRM, though it assumes a weaker Gaussian prior for W_p with a shared spatial covariance across subjects. It also assumes that all subjects share the same temporal noise covariance in addition to the shared response S . We show results for this analysis in Figure 8 in Appendix A.2.

The SRM- and MN-SRM-derived point estimates are qualitatively similar to those obtained with NTFA, but do not provide any notion of uncertainty. This makes them difficult to interpret, particularly in cases with few stimulus categories such as the Lepping and Haxby datasets.

4.6 Multivoxel Pattern and Functional Connectivity Analysis

One of the advantages of learning a deep generative model is that we can use the learned latent representations in downstream tasks. To illustrate this use case, we consider two types of post-scan analyses that are commonly performed on full fMRI data. As features in these analyses we use the low-dimensional representation learned by NTFA: the inferred factor locations, widths, and weights.

Multivoxel Pattern Analysis (MVPA): In MVPA, a regularized linear classifier is trained to predict experimental variables from distributed patterns of mean voxel intensities. This is usually preceded by a supervised feature selection step to select voxels most relevant to the classification task [Pereira et al., 2009]. We apply this standard method to our datasets and compare it to using time-averaged weight matrices derived without supervision from NTFA and HTFA. We show the resulting classification accuracy scores, measured using Area Under the (receiver operating) Curve (AUC) on the left in Figure 4. While all three methods perform significantly better than chance, NTFA outperforms HTFA, and performs almost as well as supervised voxel selection. We also note that the stimulus embeddings

qualitatively predict classification performance on different stimulus categories, as seen in the middle of Figure 4 for Lepping dataset. NTFA learns a latent representation useful for MVPA stimulus classification, without supervision. We detail the methods and results in Appendix A.9.

Functional Connectivity (FC): Functional connectivity analyses study the co-activation of brain areas during resting-state or during a task, regardless of their apparent physical distance. A variety of studies have shown FC, and changes in FC, to correlate with behavior [Elliott et al., 2019]. Voxels, however, capture neither single neurons, nor functional brain regions that could hypothetically share an activation pattern. NTFA’s latent factor representations provide a data-driven alternative to standard regions of interest (ROIs) that maintains the spatial locality crucial to functional connectivity. In Figure 4 (right), we see that linear classifiers trained on NTFA’s latent factor representations perform better at a stimulus classification task than those trained on ROIs. NTFA-derived FC patterns perform comparably to HTFA-derived patterns, despite NTFA’s lower parameter count.

5 Conclusion

We have introduced Neural Topographic Factor Analysis, an unsupervised model for fMRI data that characterizes individual variation in the neural response by inferring low-dimensional embeddings for participants and stimuli. NTFA is a first step in a line of approaches that employ deep generative models to incorporate inductive biases into unsupervised analyses of neuroimaging experiments. By designing models whose structure reflects a particular experimental design, or potentially even a neuroscientific hypothesis, we can hope to appropriately account for the uncertainties that arise from limitations in statistical power and sample sizes. This provides a path towards analyses that reason about individual variation in a manner that is data-efficient and mitigates risks of overfitting the data.

Broader Impact

While this paper reports on NTFA in terms of its characteristics as a general-purpose machine learning method for the analysis of neuroimaging data, we envision downstream impacts in the context of specific neuroscientific research questions. There is a need in neuroscience research to develop formal computational approaches that capture individual differences in neural function.

The embedding space yields a simple, visualizable model to inspect individual differences that has the potential to, at least in a qualitative manner, provide insights into fundamental questions in cognitive neuroscience. One such question is whether neural responses to stimuli are shared across individuals, vary by pre-defined participants groups (e.g. depressed vs. non-depressed participants), or are unique to participants or subgroups (e.g. as suggested by calls for “precision medicine” approaches).

Going forward, we will use our pilot data to address whether the neural basis of fear, for example, is shared across individuals and situations (i.e. there is a single “biomarker” or “neural signature” for fear), or as we expect, whether it varies by person or situation (suggesting that biomarkers for fear are idiographic) [Satpute and Lindquist, 2019]. With further developments, we plan to perform more extensive neuroimaging experiments that probe individual variation in additional fMRI datasets including in house datasets and publicly available datasets. Our hope is that the work presented in this paper will form a basis for developing probabilistic factor-analysis models with structured priors that will allow testing and development of specific neuroscientific hypotheses regarding individual variation in the functional neural organization of psychological processes.

Acknowledgments and Disclosure of Funding

The authors thank the anonymous reviewers for their constructive feedback. We also thank Jeremy Manning for insightful conversations, and Michael Shvartsman for sharing his Matrix-Normal SRM code with us. This work was supported by startup funds from Northeastern University and the University of Oregon, as well as the Intel Corporation, the National Science Foundation (NCS 1835309), and the US Army Research Institute for the Behavioral and Social Sciences (ARI W911N-16-1-0191).

References

- Hervé Abdi and Lynne J. Williams. Principal component analysis. *Wiley interdisciplinary reviews: computational statistics*, 2(4):433–459, 2010.
- Alexandre Abraham, Fabian Pedregosa, Michael Eickenberg, Philippe Gervais, Andreas Mueller, Jean Kossaifi, Alexandre Gramfort, Bertrand Thirion, and Gaël Varoquaux. Machine learning for neuroimaging with scikit-learn. *Frontiers in neuroinformatics*, 8:14, 2014.
- Geoffrey Karl Aguirre, E Zarahn, and M D’esposito. The variability of human, bold hemodynamic responses. *Neuroimage*, 8(4):360–369, 1998.
- Anna Blumenthal, Bobby Stojanoski, Chris B. Martin, Rhodri Cusack, and Stefan Köhler. Animacy and real-world size shape object representations in the human medial temporal lobes. *Human Brain Mapping*, 39(9):3779–3792, 2018. doi: 10.1002/hbm.24212. URL <https://onlinelibrary.wiley.com/doi/abs/10.1002/hbm.24212>.
- Yuri Burda, Roger Grosse, and Ruslan Salakhutdinov. Importance Weighted Autoencoders. In *International Conference on Learning Representations*, 2016. URL <http://arxiv.org/abs/1509.00519>.
- Ming Bo Cai, Michael Shvartsman, Anqi Wu, Hejia Zhang, and Xia Zhu. Incorporating structured assumptions with probabilistic graphical models in fmri data analysis. *Neuropsychologia*, 144:107500, 2020. ISSN 0028-3932. doi: <https://doi.org/10.1016/j.neuropsychologia.2020.107500>. URL <http://www.sciencedirect.com/science/article/pii/S0028393220301706>.
- Po-Hsuan Cameron Chen, Janice Chen, Yaara Yeshurun, Uri Hasson, James Haxby, and Peter J. Ramadge. A reduced-dimension fMRI shared response model. In *Advances in Neural Information Processing Systems*, pages 460–468, 2015.
- Henk R Cremers, Tor D Wager, and Tal Yarkoni. The relation between statistical power and inference in fMRI. *PLOS ONE*, 12(11):1–20, 2017. doi: 10.1371/journal.pone.0184923. URL <https://doi.org/10.1371/journal.pone.0184923>.
- Maxwell Elliott, Annchen Knodt, David Ireland, Meriwether Morris, Richie Poulton, Sandhya Ramrakha, Maria Sison, Terrie Moffitt, Avshalom Caspi, and Ahmad Hariri. What is the Test-Retest Reliability of Common Task-fMRI Measures? New Empirical Evidence and a Meta-Analysis. *Biological Psychiatry*, 87(9):S132–S133, may 2020. ISSN 0006-3223. doi: 10.1016/j.biopsych.2020.02.356. URL <https://doi.org/10.1016/j.biopsych.2020.02.356>.
- Maxwell L. Elliott, Annchen R. Knodt, Megan Cooke, M. Justin Kim, Tracy R. Melzer, Ross Keenan, David Ireland, Sandhya Ramrakha, Richie Poulton, Avshalom Caspi, Terrie E. Moffitt, and Ahmad R. Hariri. General functional connectivity: Shared features of resting-state and task fMRI drive reliable and heritable individual differences in functional brain networks. *NeuroImage*, 189:516–532, 2019. ISSN 10959572. doi: 10.1016/j.neuroimage.2019.01.068.
- Oscar Esteban, Christopher J Markiewicz, Ross W Blair, Craig A Moodie, A Ilkay Isik, Asier Erramuzpe, James D Kent, Mathias Goncalves, Elizabeth DuPre, Madeleine Snyder, et al. fmriprep: a robust preprocessing pipeline for functional mri. *Nature methods*, 16(1):111–116, 2019.
- Samuel J Gershman, David M Blei, Francisco Pereira, and Kenneth A Norman. A topographic latent source model for fmri data. *NeuroImage*, 57(1):89–100, 2011.
- Samuel J. Gershman, David M. Blei, Kenneth A. Norman, and Per B. Sederberg. Decomposing spatiotemporal brain patterns into topographic latent sources. *NeuroImage*, 98:91–102, 2014. ISSN 10959572. doi: 10.1016/j.neuroimage.2014.04.055.
- James V Haxby, M Ida Gobbini, Maura L Furey, Alumit Ishai, Jennifer L Schouten, and Pietro Pietrini. Distributed and Overlapping Representations of Faces and Objects in Ventral Temporal Cortex. *Science*, 293(5539):2425–2430, 2001. ISSN 0036-8075. doi: 10.1126/science.1063736. URL <https://science.sciencemag.org/content/293/5539/2425>.

- James V. Haxby, J. Swaroop Guntupalli, Andrew C. Connolly, Yaroslav O. Halchenko, Bryan R. Conroy, M. Ida Gobbini, Michael Hanke, and Peter J. Ramadge. A common, high-dimensional model of the representational space in human ventral temporal cortex. *Neuron*, 72(2):404–416, 2011.
- Aapo Hyvärinen, Juha Karhunen, and Erkki Oja. *Independent Component Analysis*. Wiley Online Library, 2001.
- Diederik P. Kingma and Jimmy Ba. Adam: A Method for Stochastic Optimization. In *International Conference on Learning Representations*, pages 1–15, 2015. URL <http://arxiv.org/abs/1412.6980>.
- Rebecca J. Lepping, Ruth Ann Atchley, Evangelia Chrysikou, Laura E. Martin, Alicia A. Clair, Rick E. Ingram, W. Kyle Simmons, and Cary R. Savage. Neural processing of emotional musical and nonmusical stimuli in depression. *PLoS ONE*, 11(6):1–23, 06 2016. doi: 10.1371/journal.pone.0156859. URL <https://doi.org/10.1371/journal.pone.0156859>.
- Jeremy R. Manning, Rajesh Ranganath, Waitsang Keung, Nicholas B. Turk-Browne, Jonathan D. Cohen, Kenneth A. Norman, and David M. Blei. Hierarchical topographic factor analysis. In *Pattern Recognition in Neuroimaging, 2014 International Workshop On*, pages 1–4. IEEE, 2014a.
- Jeremy R. Manning, Rajesh Ranganath, Kenneth A. Norman, and David M. Blei. Topographic Factor Analysis: A Bayesian Model for Inferring Brain Networks from Neural Data. *PLoS ONE*, 9(5): e94914, May 2014b. ISSN 1932-6203. doi: 10.1371/journal.pone.0094914.
- Jeremy R Manning, Xia Zhu, Theodore L Willke, Rajesh Ranganath, Kimberly Stachenfeld, Uri Hasson, David M Blei, and Kenneth A Norman. A probabilistic approach to discovering dynamic full-brain functional connectivity patterns. *NeuroImage*, 2018.
- Arthur Mensch, Julien Mairal, Danilo Bzdok, Bertrand Thirion, and Gaël Varoquaux. Learning neural representations of human cognition across many fmri studies. In *Advances in Neural Information Processing Systems*, pages 5883–5893, 2017.
- Siddharth Narayanaswamy, T. Brooks Paige, Jan-Willem van de Meent, Alban Desmaison, Noah Goodman, Pushmeet Kohli, Frank Wood, and Philip Torr. Learning Disentangled Representations with Semi-Supervised Deep Generative Models. In I. Guyon, U. V. Luxburg, S. Bengio, H. Wallach, R. Fergus, S. Vishwanathan, and R. Garnett, editors, *Advances in Neural Information Processing Systems 30*, pages 5927–5937. Curran Associates, Inc., 2017.
- Thomas Naselaris, Dustin E. Stansbury, and Jack L. Gallant. Cortical representation of animate and inanimate objects in complex natural scenes. *Journal of Physiology-Paris*, 106(5):239 – 249, 2012. ISSN 0928-4257. doi: <https://doi.org/10.1016/j.jphysparis.2012.02.001>. URL <http://www.sciencedirect.com/science/article/pii/S092842571200006X>. New trends in neurogeometrical approaches to the brain and mind problem.
- Francisco Pereira, Tom Mitchell, and Matthew Botvinick. Machine learning classifiers and fMRI: a tutorial overview. *NeuroImage*, 45(1 Suppl):S199–S209, 2009. ISSN 10959572. doi: 10.1016/j.neuroimage.2008.11.007. URL <http://dx.doi.org/10.1016/j.neuroimage.2008.11.007>.
- Ajay B. Satpute and Kristen A. Lindquist. The default mode network’s role in discrete emotion. *Trends in cognitive sciences*, pages 851–864, 2019.
- Michael Shvartsman, Narayanan Sundaram, Mikio Aoi, Adam Charles, Theodore Willke, and Jonathan Cohen. Matrix-normal models for fmri analysis. In *International Conference on Artificial Intelligence and Statistics*, pages 1914–1923. PMLR, 2018.
- George Tucker, Dieterich Lawson, Shixiang Gu, and Chris J. Maddison. Doubly Reparameterized Gradient Estimators for Monte Carlo Objectives. In *International Conference on Learning Representations*, pages 1–12, 2019. URL <http://arxiv.org/abs/1810.04152>.
- Tor D Wager, Jian Kang, Timothy D Johnson, Thomas E Nichols, Ajay B Satpute, and Lisa Feldman Barrett. A bayesian model of category-specific emotional brain responses. *PLoS computational biology*, 11(4), 2015.

A Appendix

Table 3: **Description of Notations.** This table explains notations used in the paper, in the order they appear in the main text.

Symbol	Description
T	Number of TRs (in a block).
V	Number of voxels in a brain image.
K	Number of factors used to approximate the input data using factor analysis (usually $K \ll V$).
$Y_n \in \mathbb{R}^{T \times V}$	n^{th} block of the dataset under analysis, organized as a number of TRs times number of voxels matrix.
$W_n \in \mathbb{R}^{T \times K}$	A lower-rank matrix of weights that specifies the time varying weights of each factor.
$F_n \in \mathbb{R}^{K \times V}$	A lower-rank matrix of factors, such that an element f_{kv} at row k and column v specifies the contribution of k^{th} factor to the activation of voxel v .
σ^Y	Gaussian noise variance, assumed constant across a given dataset.
$\mu_{n,k}^w, \sigma_{n,k}^w$	Mean and variance for k^{th} row of W_n .
μ^w, σ^w	Hyperparameters for $\mu_{n,k}^w, \sigma_{n,k}^w$.
$x_v^G \in \mathbb{R}^3$	Coordinates for voxel v .
$x_{n,k}^F \in \mathbb{R}^3, \rho_{n,k}^F$	center and log-width of the k^{th} factor for block n .
$\kappa(x_v^G, x_{n,k}^F; \rho_{n,k}^F)$	Radial basis function with center at $x_{n,k}^F$ and log-width $\rho_{n,k}^F$ evaluated at location x_v^G .
x^F, ρ^F	Hyperparameters for factor centers and factor log-widths.
P	Total number of participants in a given dataset.
S	Total number of unique stimuli in a given dataset.
$p_n \in \{1, \dots, P\}$	Participant involved in block n .
$s_n \in \{1, \dots, S\}$	Stimulus involved in block n .
$z_p^p \in \mathbb{R}^D$	D -dimensional participant embedding associated with a specific participant p .
$z_s^s \in \mathbb{R}^D$	D -dimensional stimulus embedding associated with a specific stimulus s .
$x_p^F \in \mathbb{R}^{K \times 3}, \rho_p^F \in \mathbb{R}^K$	Factor centers and log-widths for a specific participant p .
$\mu_p^x \in \mathbb{R}^{K \times 3}, \sigma_p^x \in \mathbb{R}^K$	Means and variances for the K factor centers for participant p .
$\mu_p^\rho \in \mathbb{R}^{K \times 3}, \sigma_p^\rho \in \mathbb{R}^K$	Means and variances for the K factor log-widths for participant p .
η_θ^F	Neural network that takes z_p^p as input and outputs $\mu_p^x, \sigma_p^x, \mu_p^\rho, \sigma_p^\rho$ for participant p .
$\mu_n^w \in \mathbb{R}^K, \sigma_n^w \in \mathbb{R}^K$	Mean and variance for each of the K rows of the matrix of weights W_n for block n .
η_θ^w	Neural network that takes a concatenation of z_p^p and z_s^s for participant p and stimulus s in block n and outputs μ_n^w and σ_n^w .
θ	Learnable parameters in the generative model, that is, the neural network weights.
λ	Learnable parameters of the variational distributions.
$\lambda_{n,t}^w$	Parameters of posterior distribution over weights $W_{n,t}$.
λ_s^s, λ_p^p	Parameters of posterior distribution over stimulus embedding z_s^s for stimulus s and participant embedding z_p^p for participant p .
$\lambda_{x_p^F}, \lambda_{\rho_p^F}$	Parameters of posterior distribution over factor centers x_p^F and factor log-widths ρ_p^F for participant p .
\tilde{Y}	Held-out validation data.

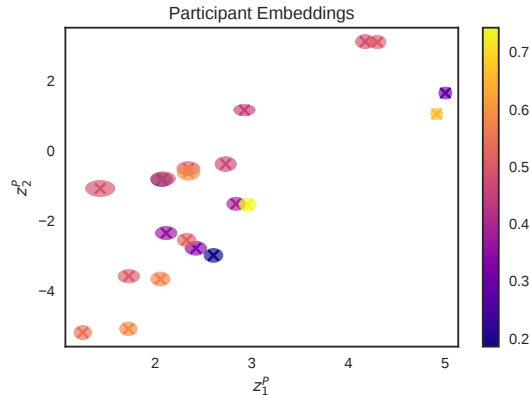


Figure 5: Participant embeddings from the ThreatVids dataset. Crosses indicate the location of the (approximate) posterior mean, and ellipses display (approximate) posterior covariance. The labels are used only for visualization purposes. Participant embeddings are color-coded by their reported level of fear across all stimulus categories (heights, spiders, and social threats). Cooler colors indicate lower mean fear ratings, while warmer colors indicate higher mean fear ratings.

A.1 Participant embedding results

In the ThreatVids dataset, the participant embeddings uncovered three groups: the more frightened, the less frightened, and those sensitive to particular fears (Figure 5). Participant embeddings for individual fear categories are shown in Figure 5. Participants were not recruited in specific groups (e.g. arachnophobes and acrophobes), and stimuli could be categorized multiple ways (e.g. by kind or degree). We observe that most participants carried a greater fear of heights (left) and social threat (right) than of spiders (middle). A scattering of individuals in the mid-left of the embedding space appeared to suffer little overall fear in any stimulus category, while those further out from the centroid had more varied fear experiences across categories. Few individuals showed high mean fear ratings across stimulus categories.

The participant embeddings do not seem to predict the self-reported fear ratings. However as shown in Figure 5 they do seem to uncover variations among participants in the latent space. Note, for example the participant groups breaking away from the central “cluster” towards top-right and bottom-left. This suggests that there are factors not explained by the self-reported fear ratings that might be driving the individual variation in response among participants.

A.2 “Embeddings” from PCA, SRM and MN-SRM

To establish a rough baseline. We performed PCA on the input data. The data Y_n from each trial n for each dataset was vectorized and these N ($T \times V$ dimensional) vectors were projected to the first two principal components. Figure 10(left) shows the result overlaid with labels for each trial. Figure 9 shows the same for the three real datasets with task labels overlaid. PCA, perhaps unsurprisingly fails to capture any meaningful structure.

We also acquired a notion of post-hoc “embeddings” from SRM and MN-SRM by following these with PCA. SRM and MN-SRM learn a single shared response matrix $S \in \mathbb{R}^{K \times T}$ for all participants in an experiment and are ideally suited to experiments where the stimuli are time aligned across participants. We mimic this structure in our datasets by artificially aligning the trials in the same order of stimuli for all participants. Then the shared response matrix was split into matrices corresponding to each stimulus. These matrices were then vectorized and PCA was done on these as mentioned before. Similarly participant embeddings can be obtained by vectorizing the participant dependent weights learned by SRM and projecting them using PCA. Figure 10(right), and Figure 10(middle) show the results of this procedure for SRM and MN-SRM on synthetic data. Similarly Figure 7 and Figure 8 show the stimulus embeddings for the three real world dataset, using SRM and MN-SRM respectively. While this procedure seems to capture reasonable embeddings for the simulated data and “ThreatVids”. We notice that a lack of uncertainty around these point estimates means it becomes

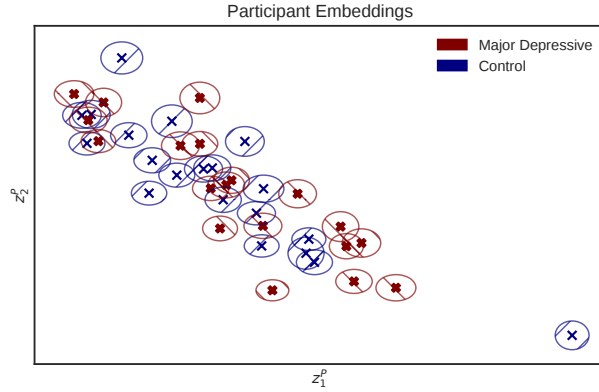


Figure 6: Participant embeddings for the Lepping dataset [Lepping et al., 2016]. Crosses indicate the location of the posterior mean, and ellipses display posterior covariance. The labels are used only for visualization purposes. Participant embeddings did not show a clear difference between control and major depressive groups, but did appear scattered around a linear trend in the latent space, which we have yet to interpret.

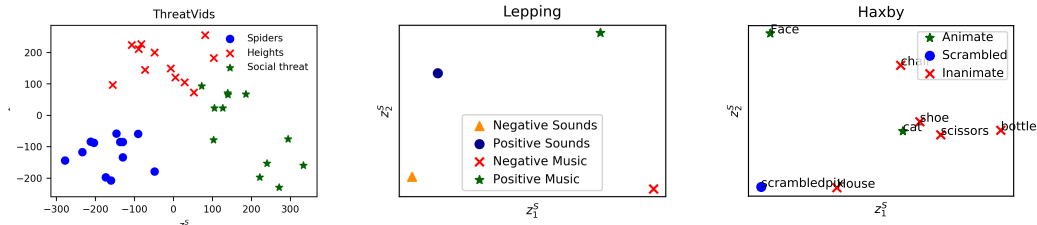


Figure 7: **Post-hoc embeddings from SRM** : Stimulus embeddings recovered post-hoc from SRM. The embeddings look qualitatively similar to NTFA, but lack uncertainty quantification which makes it difficult to meaningfully reason about the distances in the space.

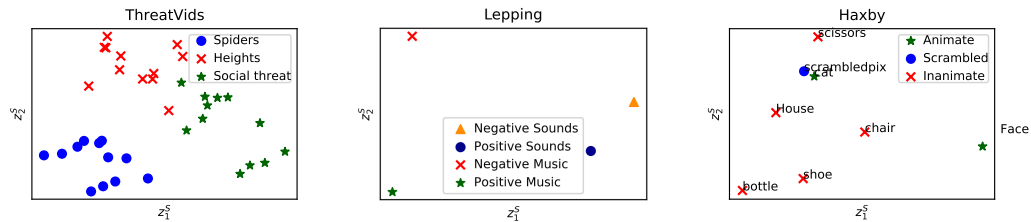


Figure 8: **Post-hoc embeddings from MN-SRM** : Stimulus embeddings recovered post-hoc from MN-SRM. The embeddings look qualitatively similar to NTFA (and SRM), but lack uncertainty quantification which makes it difficult to meaningfully reason about the distances in the space.

difficult to interpret them, specially in situations where there's only a limited number of unique stimuli. As is the case for Lepping and Haxby in the middle and right of Figure 7 and Figure 8.

A.3 Test-set predictions

To visualize the predictive distribution, we compare the time-average of \tilde{Y} to a prediction $\bar{Y} = \bar{\mu}^w \cdot \kappa(\bar{\mu}_p^x, \bar{\mu}_p^\rho)$, where $\bar{\mu}^w, \bar{\mu}^x, \bar{\rho}_p^x, \bar{\rho}_p^\rho$ are computed from the expected values \bar{z}^p and \bar{z}^s of the embeddings in the variational distribution.

Here we show test predictions from both NTFA and HTFA for our real datasets, ThreatVids (Figure 11), Lepping (Figure 12) and Haxby (Figure 13). HTFA's pale experiment-wide averages on the Lepping dataset show its inability to capture the participant- and stimulus-wise variations captured

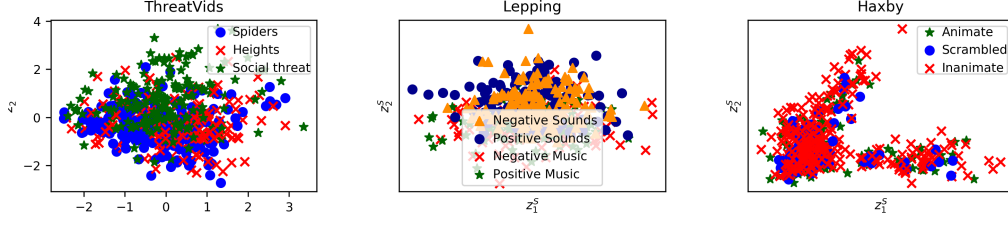


Figure 9: **PCA projections of input data as embeddings** The baseline embeddings recovered directly from input data by projecting each trial to the first two principal components. The embeddings don't seem to capture any meaningful structure.

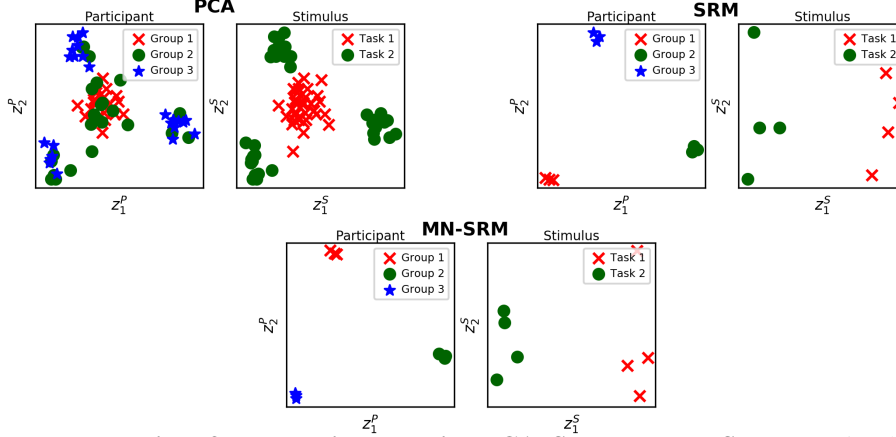


Figure 10: **Embeddings for synthetic data using PCA, SRM and MN-SRM:** On simulated data PCA fails to capture the participant or stimulus groups accurately. Post-hoc embeddings from the SRM and MN-SRM look qualitatively similar to NTFA albeit without uncertainty estimates.

clearly by NTFA. While HTFA does make clear predictions for its average across the Haxby dataset, nonetheless, it does not capture the variation across trials that NTFA does.

A.4 Derivation of the lower bound to the log posterior predictive distribution

We begin by showing how to use the variational distribution to approximate the posterior predictive distribution via importance sampling, and then convert the resulting importance weight into a lower bound on the log posterior predictive. Posterior sampling from the NTFA generative model, conditioned upon the posterior distribution over embeddings, would yield the joint distribution

$$p(\tilde{Y}, \tilde{W}, \tilde{x}^F, \tilde{\rho}^F, z^P, z^S | Y) = p(\tilde{Y}, \tilde{W}, \tilde{x}^F, \tilde{\rho}^F | z^P, z^S) p(z^P, z^S | Y),$$

which factorizes according to the generative model as,

$$p(\tilde{Y}, \tilde{W}, \tilde{x}^F, \tilde{\rho}^F, z^P, z^S | Y) = p(\tilde{Y} | \tilde{W}, \tilde{x}^F, \tilde{\rho}^F, z^P, z^S) p(\tilde{W} | z^P, z^S) p(\tilde{x}^F, \tilde{\rho}^F | z^P) p(z^P, z^S | Y).$$

The marginal of this joint distribution, that being the posterior predictive distribution, can be defined by importance weighting, where the learned variational distributions $q(z^P)$, $q(z^S)$ serve as proposals for z^P and z^S while the generative model serves as its own proposal for the other latent variables, yielding

$$\begin{aligned} p(\tilde{Y} | Y) &= \mathbb{E}_{q,p} \left[\frac{p(\tilde{Y}, \tilde{W}, \tilde{x}^F, \tilde{\rho}^F, z^P, z^S | Y)}{p(\tilde{W}, \tilde{x}^F, \tilde{\rho}^F | z^P, z^S) q(z^P) q(z^S)} \right] \\ &= \mathbb{E}_{q,p} \left[\frac{p(\tilde{Y} | \tilde{W}, \tilde{x}^F, \tilde{\rho}^F, z^P, z^S) p(\tilde{W} | z^P, z^S) p(\tilde{x}^F, \tilde{\rho}^F | z^P) p(z^P, z^S | Y)}{p(\tilde{W} | z^P, z^S) p(\tilde{x}^F, \tilde{\rho}^F | z^P) q(z^P) q(z^S)} \right] \\ &= \mathbb{E}_{q,p} \left[\frac{p(\tilde{Y} | \tilde{W}, \tilde{x}^F, \tilde{\rho}^F, z^P, z^S) p(z^P, z^S | Y)}{q(z^P) q(z^S)} \right]. \end{aligned}$$

We can then apply Jensen’s inequality to define a lower bound

$$\begin{aligned} & \text{ELBO}_{\tilde{Y}|Y} \\ &= \mathbb{E}_{q,p} \left[\log \frac{p(\tilde{Y} | \tilde{W}, \tilde{x}^F, \tilde{\rho}^F, z^P, z^S) p(z^P, z^S | Y)}{q(z^P) q(z^S)} \right] \\ &\leq \log p(\tilde{Y} | Y). \end{aligned}$$

This is a standard definition of the ELBO, albeit for the posterior predictive distribution rather than the marginal likelihood (i.e. the prior predictive). By converting the log of a product of densities into a sum of log-density terms and noting that the expectations are over proposal distributions $p = p(\tilde{W}, \tilde{x}^F, \tilde{\rho}^F | z^P, z^S)$ and $q = q(z^P) q(z^S)$, we can write this ELBO as:

$$\begin{aligned} \text{ELBO}_{\tilde{Y}|Y} &= \mathbb{E}_{q,p} \left[\log p(\tilde{Y} | \tilde{W}, \tilde{x}^F, \tilde{\rho}^F, z^P, z^S) - \log \frac{q(z^P)q(z^S)}{p(z^P, z^S | Y)} \right] \\ \text{ELBO}_{\tilde{Y}|Y} &= \mathbb{E}_{q,p} \left[\log p(\tilde{Y} | \tilde{W}, \tilde{x}^F, \tilde{\rho}^F, z^P, z^S) \right] - \text{KL}(q(z^P) q(z^S) || p(z^P, z^S | Y)), \end{aligned}$$

From the standard decomposition of the ELBO we can also reason that,

$$\text{ELBO}_{\tilde{Y}|Y} = \log p(\tilde{Y} | Y) - \text{KL}(q(z^P) q(z^S) || p(z^P, z^S | \tilde{Y}, Y)),$$

and therefore

$$\begin{aligned} \mathbb{E}_{q,p} \left[\log p(\tilde{Y} | \tilde{W}, \tilde{x}^F, \tilde{\rho}^F, z^P, z^S) \right] - \text{KL}(q(z^P) q(z^S) || p(z^P, z^S | Y)) &= \\ \log p(\tilde{Y} | Y) - \text{KL}(q(z^P) q(z^S) || p(z^P, z^S | \tilde{Y}, Y)), & \\ \mathbb{E}_{q,p} \left[\log p(\tilde{Y} | \tilde{W}, \tilde{x}^F, \tilde{\rho}^F, z^P, z^S) \right] = \log p(\tilde{Y} | Y) & \\ - \text{KL}(q(z^P) q(z^S) || p(z^P, z^S | \tilde{Y}, Y)) & \\ + \text{KL}(q(z^P) q(z^S) || p(z^P, z^S | Y)). & \end{aligned}$$

Since the variational distributions q were already optimized during training to minimize the KL divergence in the third term on the right hand side of the above equation, we can reason that it will be small compared to the KL divergence in the second term (between the variational distribution and the true posterior given the test data). The difference of KL’s should therefore remain nonnegative, allowing us to use the expected log-likelihood as a lower bound to the log posterior predictive probability of the test data. Additionally, the low dimensionality ($D = 2$ in our experiments) of z^P and z^S compared to Y led the log likelihood to dominate the ELBO in all our experiments, a fact which should not be changed by passing to $\text{ELBO}_{\tilde{Y}|Y}$. This leads to Equation (11) in Section 4.

A.5 Description of datasets

Threat Videos (“ThreatVids”)⁴: A fundamental question in affective neuroscience is whether threat-relevant stimuli from different categories involve a single or multiple distinct systems [Wager et al., 2015]. To evaluate whether NTFA can provide insight into this fundamental research question, we conducted and analyzed our own study. 21 participants each watched 36 videos depicting threat-related content involving spiders, looming heights, and social evaluative threat (12 videos per category). Each video was approximately 20 seconds long and was followed by a set of self-report ratings and a rest period. The videos were chosen to vary in how much fear they normatively evoke within each category. This data contains 81,638 voxels (white matter removed) and 552 time points per scanning run for three runs. Using NTFA, we examine whether neural activity justified organization of the stimuli into three categories.

⁴This dataset is currently in preparation for online repository pending deidentification and submission of an empirical report.

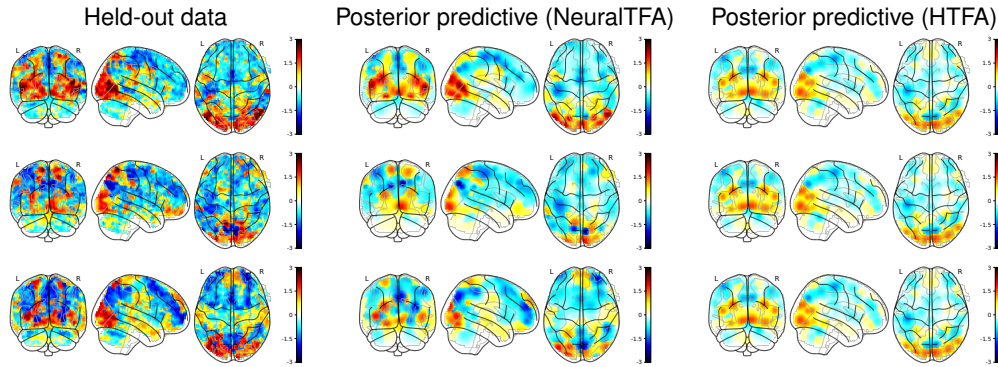


Figure 11: **Test predictions for the ThreatVids dataset:** We compare time-averaged held-out data (*left*) to the posterior-predictive mean for three trials. In NTFA (*center*), the learned generative model and inferred embeddings inform the distribution for unseen participant-stimulus combinations. In HTFA (*right*) the predictive distribution is the same for trials, since the shared global template in this model does not differentiate between participants and stimuli.

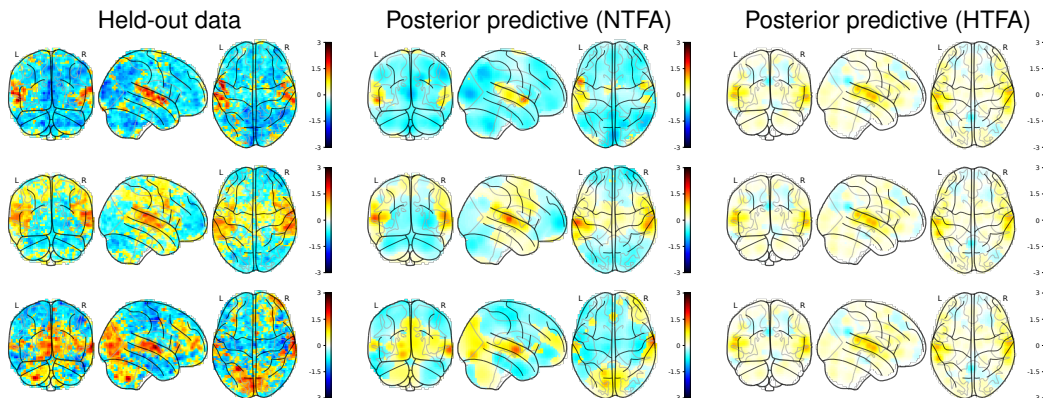


Figure 12: **Test predictions for the Lepping dataset:** We show average images for three trials, with participant-stimulus pairs held out from the training set. Posterior predictive estimates under NTFA (*center*) capture meaningful trial-specific variation in the original images (*left*), whereas HTFA can only re-use its same global template across differing trials (*right*).

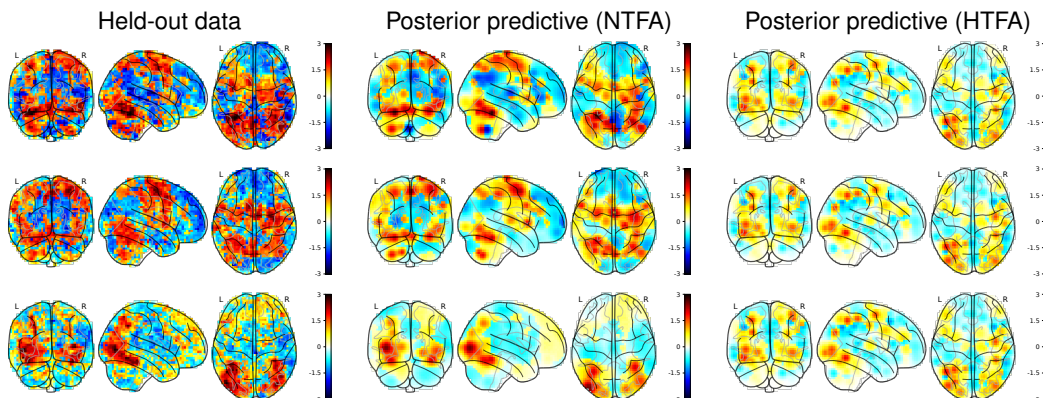


Figure 13: **Test predictions for the Haxby dataset:** We show average images for three trials, with participant-stimulus pairs held out from the training set. Posterior predictive estimates under NTFA (*center*) capture meaningful trial-specific variation in the original images (*left*), whereas HTFA can only re-use its same global template across differing trials (*right*).

Emotional Musical and Nonmusical Stimuli in Depression (“Lepping”) [Lepping et al., 2016]⁵: 19 participants with major depressive disorder and 20 control participants (P=39) underwent musical and nonmusical stimuli to examine neural processing of emotionally provocative auditory stimuli in depression. In each trial, participants listened to music or nonmusical valenced (positive or negative) sounds, interleaved with trials in which they heard neutral tones. The fMRI data had 62,733 voxels (white matter removed) and 105 time points in each scanning run for five runs.

Face and Objects Image Viewing (“Haxby”) [Haxby et al., 2001]⁶: fMRI was used to measure whole brain response while subjects viewed faces, cats, five categories of man-made objects, and scrambled pictures. The study consisted of six subjects (P=6) and 12 scanning runs per subject, with 32,233 voxels (white matter removed) and 121 time points for each scanning run.

Table 4: Dataset Summary

	No. Participants	No. of Stimuli	TRs per block	No. of Voxels
	P	S	T	V
Synthetic	9	8	20	5,000
ThreatVids	23	36	20	81,638
Lepping	39	4	10	62,733
Haxby	6	8	12	32,233

A.6 Preprocessing

The raw BOLD signal collected in fMRI is generally not usable for analysis. It contains both physiological (cerebrospinal fluids, global signal, and white matter) and motion artifacts. We employ standard neuroimaging preprocessing - including slice timing correction, high pass filtering and spatial smoothing - for all fMRI data using fMRIPrep [Esteban et al., 2019]. The processed data still has units that are incomparable across scanning runs. For the ThreatVids and Haxby datasets, we z-scored each task trial with respect to the entire set of rest trials (trials in which no stimulus was presented) within each run. For the Lepping dataset, we treated neutral tones as rest trials and performed the same z-scoring procedure. This provides a common scale of units across trials within a dataset, capturing meaningful difference in activation intensities relative to neutral conditions (“rest” and “tones”). Since neural activity peaks about three seconds after the task onset [Aguirre et al., 1998], we make sure to account for this delay when loading each dataset by offsetting the stimulus onsets by three seconds. We input the resulting z-scored data to NTFA, and use it for all evaluations.

A.7 Neural network architectures and initialization

The network $\eta_{\theta}^f(\cdot)$ is a multilayer perceptron (MLP) with one hidden layer and PReLU activations. We extract the factor parameters F , x and F , ρ by viewing the $8K$ -dimensional result as a $K \times 4 \times 2$ tensor. The network $\eta_{\theta}^w(\cdot)$ is similarly an MLP with one hidden layer, though operating over both embeddings. We extract the weight parameters w_n by casting its $2K$ -dimensional result as a $K \times 2$ matrix. Architectural details for both networks are given in Table 5. The neural network weights θ specify the linear layers of the networks.

We train the parameters θ and λ on all models using the Adam optimizer [Kingma and Ba, 2015] for 1000-1500 epochs per dataset. We use one particle to calculate the IWAE-style bound to the log-evidence and its gradient estimator at training time, with a learning rate $\eta_{\lambda} = 0.01$ and $\eta_{\theta} = 0.0001$. We anneal the learning rate with a patience of 100 epochs, and a multiplicative decline of 0.5.

Similarly to Manning et al. [2018], we employ a K-means initialization in all experiments across models, initializing the variational parameters for HTFA and the bias in the final layer of the generative model for NTFA.

⁵This data was obtained from the OpenfMRI database. Its accession number is ds000171.

⁶<https://openneuro.org/datasets/ds000105/>

Table 5: Network architectures for η_θ^F and η_θ^W

Layer	$p_\theta(x_p^F, \rho_p^F z_p^F)$	$p_\theta(W_{n,t} z_p^F, z_s^S)$
Input	$z_p^F \in \mathbb{R}^D$	$z_p^F, z_s^S \in \mathbb{R}^D$
1	FC $D \times 2D$ PReLU	FC $2D \times 4D$ PReLU
2	FC $2D \times 4D$ PReLU	FC $4D \times 8D$ PReLU
3	FC $4D \times 8K$	FC $8D \times 2K$
Output	$(\mu_p^x, \sigma_p^x, \mu_p^\rho, \sigma_p^\rho) \in \mathbb{R}^{8K}$	$(\mu_n^W, \sigma_n^W) \in \mathbb{R}^{2K}$

A.8 Synthetic data generation

We consider a simulated dataset in which there are three participant groups (*Group 1*, *Group 2* and *Group 3*) of three participants each. All participants underwent two categories of hypothetical stimuli, called *Task 1* and *Task 2*, with four stimuli within each category. Each participant underwent one hypothetical scanning run with rest trials interleaved between stimuli. We manually defined three distinct factors in a standard MNI_152_8mm brain. We then sampled participant embeddings $\{z_1^p, \dots, z_9^p\}$ and stimulus embeddings $\{z_1^s, \dots, z_8^s\}$, from mixtures of three and two distinct Gaussians respectively. We set the means for these Gaussians to meet the following conditions under noisy combination. **1.** All participants show no whole-brain response during rest except random noise. **2.** Under *Task 1* stimuli, Group 1 exhibits approximately half the response in the first region as compared to under *Task 2* stimuli. The rest of the brain shows no response. Similarly, Group 2 and Group 3 exhibit a response in the second and third regions respectively, while the rest of the brain shows no response. **3.** Each stimulus in *Task 1* and *Task 2* provokes a response lower or higher than the stimulus category’s average based on the stimulus embedding’s location. Algorithm 2 shows the pseudocode for generating synthetic datasets similar to this synthetic data used in this paper. We will also include the exact script with the code repository for our method.

Algorithm 2 Generating a simple Synthetic data to test NTFA using Nilearn [Abraham et al., 2014]. For a dataset with T time points per block, K factors, C stimulus categories, N_C stimuli per category, G participant groups, and N_G participants per group. This leads to $S = C * N_C + (2N_C + 1)$ stimuli (to allow for interleaved rest blocks) and $P = G * N_G$ participants.

```

1: Load Template Brain ▷ e.g. MNI_152_8mm
2: Define  $\mu_{1\dots C}^S, \Sigma_{1\dots C}^S$  ▷ means and covariances for embeddings for each stimulus category.
3: Define  $\mu_{1\dots G}^P, \Sigma_{1\dots G}^P$  ▷ means and covariances for each participant group.
4:  $x_{1,\dots,K}^F \leftarrow K$  ▷ manually selected voxels.
5: Define  $\sigma^x, \mu^\rho, \sigma^\rho$  ▷ variance for factor centers, means and variance for log-width
6:  $\rho_{1,\dots,K} \sim \mathcal{N}(\mu^\rho, \sigma^\rho)$ 
7:  $F \leftarrow \text{RBF}(x, \rho)$  ▷ create factor matrix using radial basis functions
   Order the total stimuli according to required experiment design and save indices accordingly.
   e.g. Category 1, Rest, Category 2, Rest, and so on.
8: for  $c$  in  $1, \dots, C$  do
9:   for  $s$  in  $1, \dots, N_C$  do  $z_s^c \sim \mathcal{N}(\mu_c^S, \Sigma_c^S)$  ▷ generate stimulus embeddings
10: for  $g$  in  $1, \dots, G$  do
11:   for  $p$  in  $1, \dots, N_G$  do  $z_p^g \sim \mathcal{N}(\mu_g^P, \Sigma_g^P)$  ▷ generate participant embeddings
12: for  $g$  in  $1, \dots, G$  do
13:   for  $p$  in  $1, \dots, N_G$  do
14:     for  $s$  in  $1, \dots, S$  do
15:       for  $k$  in  $1, \dots, K$  do
16:          $W_{[k,s:s+T]} \sim \mathcal{N}(0, \sigma^W)$  ▷ if  $s$  is the start of a rest block
17:          $W_{[k,s:s+T]} \sim \mathcal{N}(z_p^T z_s, \sigma^W)$ 
    $Y_{p+(g-1)*N_G} = WF$  ▷ data for one participant

```

A.9 MVPA Classification

In this section we provide details of the classification pipeline as well as results beyond those presented in Figure 4. The traditional pipeline outlined in Pereira et al. [2009] was used to do classification on the input data. One classical approach is to first select a subset of voxels with reliably different mean intensities between the experimental variables being tested. Usually this is done by selecting 500 voxels based on the f -statistic from an analysis of variance (ANOVA). After this supervised feature selection step, a linear support-vector machine (SVM) is usually trained (without hyperparameter tuning) over some combination of cross-validation scans.

For each block (an instance of a participant undergoing a stimulus), only the mean voxel activity was considered. We employed a leave-out-one cross-validation approach with respect to scanning runs for each subject, with a one-vs-all linear SVM trained and tested for each stimulus category. For Haxby and ThreatVids, we used a leave-one-out cross-validation approach on scanning runs, while for Lepping (in which the experimental design did not support leaving whole scanning sessions out) we applied a stratified three-fold cross-validation scheme across all trials with the same stimulus. We then ran the same classification pipeline again, substituting NTFA’s and HTFA’s MAP estimates of the weight matrix W for the label-supervised voxels.

For each cross validation run, the feature selection of voxels was done by keeping the top 500 of the voxels with the most reliable differences in the mean intensity for the stimulus category the classifier was being trained for vs the remaining categories. The linear SVM trained on these selected voxels on training runs was then tested on the held-out runs. Since this is a one-vs-all scheme, the classes are unbalanced, and raw accuracy can be inflated just by predicting the most frequent class. We therefore report Area Under the ROC Curve (AUC) instead.

For NTFA and HTFA, we use the same pipeline, except there is no supervised feature selection step. Instead, we used MAP estimates of generated $W \in \mathbb{R}^{T \times K}$ matrices, averaged across time. These were employed as the training features for classifiers with respect to the cross-validation scheme above. As is evident from Figure 4, and Tables 6 and 7, NTFA performs similarly to the supervised pipeline above, and often outperforms HTFA.

Based on suggestion from a reviewer, we also considered including NTFA training within the cross validation folds. However, we note that this is computationally very expensive, since MVPA here is done with separate cross-validation folds for each subject. This would result in training NTFA more than 50 times for the three real datasets. Moreover, given the unsupervised nature of NTFA, we believe that this shortcut of training NTFA on all data only once to extract features is unlikely to be problematic.

Table 6: **Classification Details** on ThreatVids dataset. “Voxel” indicates the ANOVA-SVM strategy on input data. NTFA performs consistently better than HTFA and closer to performing a completely supervised feature selection + classification pipeline on the input data.

Subject	Voxel			NTFA			HTFA		
	Heights	Social	Spiders	Heights	Social	Spiders	Heights	Social	Spiders
4	.90 ± .03	.94 ± .04	.96 ± .06	.86 ± .01	.89 ± .09	1.00 ± .00	.84 ± .07	.90 ± .10	.86 ± .06
5	.91 ± .08	.97 ± .03	1.00 ± .00	.85 ± .03	.91 ± .11	.97 ± .03	.58 ± .10	.62 ± .17	.76 ± .15
6	.42 ± .08	.26 ± .09	.54 ± .08	.45 ± .11	.27 ± .06	.61 ± .09	.30 ± .14	.35 ± .13	.58 ± .15
7	.44 ± .03	.38 ± .06	.39 ± .05	.44 ± .00	.44 ± .09	.36 ± .00	.59 ± .06	.25 ± .00	.30 ± .11
8	.99 ± .01	.86 ± .10	1.00 ± .00	.96 ± .01	.91 ± .05	.99 ± .01	.79 ± .10	.80 ± .04	.96 ± .03
9	.56 ± .17	.46 ± .05	.57 ± .15	.52 ± .12	.36 ± .06	.42 ± .13	.74 ± .10	.77 ± .16	.64 ± .10
10	.97 ± .04	.96 ± .03	1.00 ± .00	.99 ± .01	.95 ± .05	1.0 ± .00	.93 ± .04	.94 ± .04	.95 ± .04
11	.86 ± .13	.93 ± .03	.94 ± .07	.85 ± .14	.90 ± .03	.86 ± .08	.66 ± .04	.84 ± .08	.69 ± .17
12	.36 ± .19	.67 ± .06	.65 ± .18	.49 ± .08	.53 ± .10	.61 ± .17	.38 ± .22	.60 ± .08	.51 ± .11
13	.88 ± .09	.99 ± .02	.85 ± .11	.91 ± .08	.98 ± .02	.86 ± .10	.80 ± .15	.87 ± .03	.86 ± .03
14	.85 ± .03	.89 ± .05	.97 ± .03	.81 ± .00	.89 ± .02	1.0 ± .00	.87 ± .03	.94 ± .03	.98 ± .01
15	.82 ± .10	.87 ± .09	.92 ± .08	.84 ± .07	.93 ± .05	.95 ± .07	.60 ± .11	.85 ± .08	.83 ± .13
16	.96 ± .03	.99 ± .01	.95 ± .01	.96 ± .03	.99 ± .01	.96 ± .03	.85 ± .11	1.0 ± .00	.93 ± .05
17	1.0 ± .00	.92 ± .05	.83 ± .07	.91 ± .04	.83 ± .04	.88 ± .04	.95 ± .02	.47 ± .12	.81 ± .15
18	.81 ± .14	.68 ± .11	.81 ± .08	.63 ± .14	.58 ± .17	.59 ± .07	.68 ± .07	.59 ± .08	.70 ± .05
19	.85 ± .01	.94 ± .04	.85 ± .09	.89 ± .03	.93 ± .00	.84 ± .08	.88 ± .04	.81 ± .04	.67 ± .14
23	.70 ± .05	.85 ± .06	.72 ± .07	.81 ± .03	.81 ± .03	.85 ± .07	.58 ± .02	.66 ± .09	.75 ± .09
25	.84 ± .06	.95 ± .03	.99 ± .01	.76 ± .04	.93 ± .07	.99 ± .01	.61 ± .12	.94 ± .02	.90 ± .04
26	.84 ± .16	.53 ± .03	.82 ± .10	.64 ± .11	.76 ± .05	.81 ± .09	.77 ± .15	.59 ± .00	.95 ± .05
28	.78 ± .07	.97 ± .03	1.0 ± .00	.96 ± .05	.97 ± .00	1.0 ± .00	.83 ± .15	.87 ± .05	.99 ± .01
29	.95 ± .07	.94 ± .04	1.0 ± .00	.87 ± .09	.93 ± .04	.93 ± .05	.90 ± .03	.95 ± .01	.95 ± .04

Table 7: **Classification Details** on Lepping dataset. “Voxel” indicates the ANOVA-SVM strategy on input data. NTFA performs consistently better than HTFA and closer to performing a completely supervised feature selection + classification pipeline on the input data.

Subject	Voxel				NTFA				HTFA			
	-Music	-Sounds	+Music	+Sounds	-Music	-Sounds	+Music	+Sounds	-Music	-Sounds	+Music	+Sounds
CTRL-1	.75 ± .20	.42 ± .43	.58 ± .24	.79 ± .12	.75 ± .20	.29 ± .21	.96 ± .06	.58 ± .31	.96 ± .06	.37 ± .27	.92 ± .12	.83 ± .24
CTRL-2	.62 ± .27	.92 ± .12	.92 ± .12	.54 ± .06	.79 ± .21	1.0 ± .00	.79 ± .16	.75 ± .20	.67 ± .31	.92 ± .12	.71 ± .21	.58 ± .24
CTRL-3	.12 ± .10	.54 ± .29	.71 ± .21	.29 ± .21	.58 ± .12	.79 ± .29	.87 ± .10	.58 ± .12	.71 ± .21	.83 ± .12	.79 ± .212	.42 ± .12
CTRL-4	.79 ± .16	.79 ± .16	.67 ± .12	.67 ± .12	.92 ± .12	.62 ± .10	.75 ± .20	.67 ± .12	.87 ± .18	.58 ± .12	.83 ± .12	.58 ± .12
CTRL-5	.71 ± .25	.54 ± .33	.83 ± .24	.62 ± .10	.67 ± .12	.67 ± .31	.87 ± .12	.62 ± .18	.75 ± .20	.67 ± .24	.83 ± .20	.83 ± .12
CTRL-6	.50 ± .41	.79 ± .16	.67 ± .24	.83 ± .24	.42 ± .24	.83 ± .12	.92 ± .12	1.0 ± .00	.58 ± .42	.75 ± .20	.96 ± .06	1.0 ± .00
CTRL-7	.79 ± .16	.42 ± .42	.58 ± .12	.50 ± .20	.92 ± .12	.42 ± .42	.33 ± .12	.25 ± .20	.83 ± .12	.46 ± .41	.50 ± .20	.17 ± .24
CTRL-8	1.0 ± .00	.83 ± .12	.86 ± .10	.75 ± .20	1.0 ± .00	.75 ± .00	1.0 ± .00	1.0 ± .00	.67 ± .12	.92 ± .12	1.0 ± .00	.92 ± .12
CTRL-9	.58 ± .12	.96 ± .06	.71 ± .21	.50 ± .00	.42 ± .31	.92 ± .12	.92 ± .12	.67 ± .12	.75 ± .00	.92 ± .12	.87 ± .10	.58 ± .24
CTRL-10	.62 ± .31	.87 ± .10	.37 ± .10	.17 ± .12	.37 ± .44	.83 ± .12	.25 ± .20	.21 ± .16	.92 ± .12	.83 ± .12	.75 ± .20	.50 ± .20
CTRL-11	.46 ± .21	.87 ± .18	.54 ± .16	1.0 ± .00	.33 ± .12	1.0 ± .00	.33 ± .12	1.0 ± .00	.58 ± .12	.79 ± .16	.50 ± .20	1.0 ± .00
CTRL-12	.83 ± .12	.67 ± .24	.87 ± .10	.92 ± .12	.75 ± .20	.67 ± .31	.83 ± .12	.71 ± .06	.75 ± .20	.58 ± .12	.79 ± .83	.83 ± .24
CTRL-13	.71 ± .26	.67 ± .31	.92 ± .12	.29 ± .26	.92 ± .12	.75 ± .35	.75 ± .20	.29 ± .26	.67 ± .24	.25 ± .20	.71 ± .21	.75 ± .20
CTRL-14	.58 ± .31	.67 ± .31	.33 ± .12	.83 ± .12	.62 ± .31	.87 ± .10	.33 ± .12	.75 ± .20	.67 ± .24	.46 ± .16	.42 ± .12	.87 ± .18
CTRL-15	.62 ± .18	.87 ± .18	.58 ± .31	.92 ± .12	.58 ± .24	.67 ± .47	.50 ± .20	.62 ± .10	.58 ± .12	.79 ± .29	.08 ± .12	.87 ± .18
CTRL-16	.87 ± .18	.79 ± .21	.46 ± .16	.58 ± .31	.92 ± .12	.67 ± .12	.33 ± .31	.50 ± .20	.87 ± .10	.83 ± .12	.50 ± .41	.42 ± .24
CTRL-17	.67 ± .31	.25 ± .20	.79 ± .16	.62 ± .10	.37 ± .10	.21 ± .21	.83 ± .12	.37 ± .27	.71 ± .26	.29 ± .26	.79 ± .16	.79 ± .21
CTRL-18	.71 ± .21	.62 ± .37	.83 ± .12	.83 ± .12	.83 ± .24	.67 ± .12	.92 ± .12	.62 ± .17	.92 ± .12	1.0 ± .00	.92 ± .12	.46 ± .33
CTRL-19	.87 ± .10	1.0 ± .00	.54 ± .36	.92 ± .12	.96 ± .06	.75 ± .202	.50 ± .41	.92 ± .12	.83 ± .24	.96 ± .06	.33 ± .24	.58 ± .24
CTRL-20	.83 ± .24	.83 ± .12	.54 ± .33	.50 ± .00	.79 ± .16	.87 ± .12	.42 ± .42	.37 ± .10	.58 ± .31	.67 ± .12	.46 ± .39	.62 ± .31
MDD-1	.54 ± .36	.75 ± .20	.83 ± .12	.08 ± .12	.79 ± .16	.75 ± .20	.833 ± .12	.17 ± .12	.67 ± .12	.67 ± .31	1.0 ± .00	.17 ± .12
MDD-2	.67 ± .24	.25 ± .00	.83 ± .24	.67 ± .31	.67 ± .31	.17 ± .12	.75 ± .20	.67 ± .31	.67 ± .47	.42 ± .24	.79 ± .29	.71 ± .06
MDD-3	.11 ± .16	1.0 ± .00	.58 ± .31	.25 ± .35	.44 ± .34	.89 ± .16	.56 ± .42	.25 ± .20	.19 ± .14	.89 ± .16	.64 ± .31	.00 ± .00
MDD-4	.79 ± .16	.62 ± .10	.75 ± .20	.83 ± .12	.83 ± .12	.58 ± .31	.75 ± .20	.75 ± .00	.71 ± .06	.67 ± .24	.54 ± .33	.87 ± .10
MDD-6	.67 ± .31	.58 ± .42	.87 ± .10	.92 ± .12	.67 ± .31	.75 ± .35	.92 ± .12	.62 ± .31	.71 ± .21	.62 ± .18	.96 ± .06	.79 ± .21
MDD-7	.54 ± .16	.79 ± .16	.42 ± .31	.58 ± .31	.54 ± .21	.83 ± .12	.75 ± .00	.62 ± .10	.62 ± .10	.58 ± .12	.71 ± .06	.42 ± .31
MDD-8	.83 ± .12	.58 ± .31	.79 ± .21	.42 ± .31	.92 ± .19	.42 ± .12	.71 ± .33	.33 ± .471	.87 ± .10	.54 ± .26	.83 ± .12	.33 ± .47
MDD-9	1.0 ± .00	.67 ± .12	.87 ± .18	.96 ± .06	1.0 ± .00	.25 ± .20	1.0 ± .00	.92 ± .12	1.0 ± .00	.29 ± .33	.75 ± .20	.83 ± .12
MDD-10	1.0 ± .00	.87 ± .18	.83 ± .24	.58 ± .12	1.0 ± .00	.92 ± .12	.83 ± .24	.50 ± .00	.92 ± .12	.87 ± .18	.79 ± .21	.71 ± .21
MDD-11	.62 ± .10	.67 ± .12	.79 ± .21	.83 ± .12	.54 ± .16	.83 ± .12	.87 ± .18	.79 ± .16	.46 ± .06	.37 ± .31	1.0 ± .00	.75 ± .20
MDD-12	.83 ± .24	.42 ± .12	.58 ± .12	.79 ± .16	.71 ± .33	.33 ± .12	.71 ± .21	.58 ± .12	.46 ± .16	.17 ± .12	.67 ± .10	.37 ± .10
MDD-13	.67 ± .31	.71 ± .26	.25 ± .00	.58 ± .12	.92 ± .12	1.0 ± .00	.42 ± .12	.58 ± .12	1.0 ± .00	.92 ± .12	.58 ± .12	.75 ± .20
MDD-14	.58 ± .24	.83 ± .12	.58 ± .31	.58 ± .12	.33 ± .12	.79 ± .16	.50 ± .20	.67 ± .31	.37 ± .10	.62 ± .10	.67 ± .12	.58 ± .24
MDD-15	1.0 ± .00	.58 ± .24	.75 ± .20	.58 ± .12	.83 ± .12	.75 ± .20	.83 ± .24	.75 ± .20	.58 ± .31	.50 ± .41	.79 ± .21	.67 ± .12
MDD-16	.92 ± .12	.46 ± .39	.29 ± .26	.37 ± .10	.96 ± .06	.46 ± .39	.54 ± .39	.54 ± .06	.96 ± .06	.62 ± .31	.42 ± .24	.37 ± .10
MDD-17	1.0 ± .00	.21 ± .06	.67 ± .24	.75 ± .20	1.0 ± .00	.25 ± .20	.50 ± .00	.83 ± .12	.87 ± .18	.25 ± .00	.79 ± .21	1.0 ± .00
MDD-18	.83 ± .24	1.0 ± .00	.75 ± .00	.92 ± .12	.83 ± .24	.33 ± .24	.92 ± .12	.92 ± .12	.42 ± .12	.29 ± .21	.83 ± .12	.58 ± .31
MDD-19	.75 ± .00	.62 ± .18	.58 ± .24	.92 ± .12	.75 ± .00	.62 ± .10	.75 ± .00	.83 ± .12	.92 ± .12	.75 ± .20	.58 ± .12	.58 ± .24